

Received October 8, 2019, accepted October 20, 2019, date of publication October 24, 2019,
date of current version November 4, 2019.

Digital Object Identifier 10.1109/ACCESS.2019.2949265

Real-Time Quadruple-Frequency Cycle Slip Detection and Repair Algorithm Based on the Four Chosen Linear Combinations

YAODING WANG¹, KE ZHANG, WENXIANG LIU, ZHENGRONG LI, AND FEIXUE WANG

College of Electronic Science, National University of Defense Technology, Changsha 410073, China

Corresponding author: Ke Zhang (zhane0915@163.com)

This work was supported in part by the National Natural Science Foundation of China under Grant 41604016.

ABSTRACT GNSS is now being speedily expanded to our daily life, but the positioning precision still can hardly meet the demands of many high-precision applications, such as approaching landing system on airports. Due to the development of GNSS, quadruple-frequency signals are now available in China's BeiDou Navigation Satellite System (BDS) and the European Galileo system, which can contribute to positioning precision. Positioning precision can not be improved obviously by quadruple-frequency carrier phases until cycle slips are detected and repaired. A method using four linear combinations to detect and repair quadruple-frequency cycle slips is proposed in the paper. The choices of the four linear combinations are conducted in cascaded steps in accordance to the cycle slip fixing probability. When the four detection combinations are determined, cycle slips on original carrier phase observations can be uniquely determined. The proposed algorithm has been tested on real 30-second quadruple-frequency static observations of BDS and Galileo and on real 0.05-second quadruple-frequency kinematic observations of BDS and Galileo. Simulated and real cycle slips are tested. The results show that the proposed algorithm can detect and repair cycle slips even for one cycle effectively.

INDEX TERMS Quadruple-frequency observations, cycle slip, linear combination, BDS, Galileo.

I. INTRODUCTION

With the completion of the experimental and regional phases, China's BeiDou Navigation Satellite System (BDS) is being speedily expanded to a global and multifunctional satellite navigation system, BDS-3 [1]. To ensure the smooth transition from BDS-2 to BDS-3, B1I and B3I will continue to be broadcast while B2I will not be retained [2]. At the same time, two new OS (open service) signals, i.e. B1C and B2a, will be broadcast by the BDS-3 satellites [3], [4]. Those four signals are broadcast on four frequencies and can be received by BDS users. In addition, the European Galileo system has broadcasted quadruple-frequency signals, i.e. E1, E5a, E5b and E6, and several researches have been done based on Galileo quadruple-frequency signals [5], [6].

Carrier phase measurements are the important observations for highly accurate positioning because of their high accuracy. Multi-frequency signals can form more linear combinations with small combined noise, small ionospheric

delay and long wavelength compared with single-frequency signal, and multi-frequency signals are used in many high precise applications, such as approaching landing system and geodetic measurement applications [7]–[18]. Cycle slips can interrupt the consistence of multi-frequency carrier phase measurements so that degrade the precise of positioning. It is necessary to detect and repair cycle slip when multi-frequency carrier phase measurements are used in high precise applications.

Over the past decades, there have been many methods to detect and repair cycle slips. Chen et al. used double differenced observations to detect and repair cycle slips which needed two receivers at least [7]. For most of applications, we can only process one receiver data so that the methods to detect and repair un-differenced cycle slips are more attractive. For dual-frequency receiver, the Hatch-Melbourne-Wubben (HMW) [8] linear combination can be applied to detect cycle slips. In addition, the difference of carrier phase observations on two frequencies, which is called as the ionospheric residual combination, can also be applied to detect cycle slips. TurboEdit algorithm uses both

The associate editor coordinating the review of this manuscript and approving it for publication was Mohsin Jamil¹.

the HMW combination and the ionospheric residual combination to detect and repair dual-frequency cycle slips [9]. Because of the ionospheric residual combination, the TurboEdit algorithm does not perform well under high ionospheric activity. In order to detect and repair cycle slip under high ionospheric activity for a dual-frequency receiver, researchers have developed several methods. A forward and backward moving window averaging algorithm and a second-order, time-difference phase ionospheric residual algorithm are used by Cai et al. to detect and repair cycle slips [10]. Liu used the ionospheric total electron contents rate (TECR) and HMW wide lane linear combination to uniquely determine the cycle slip on both L1 and L2 frequencies [11]. Banville et al. proposed a geometry-based approach with the rigorous handling of the ionosphere [12]. Triple-frequency signals are now available and many researches have been done with triple-frequency signals. Hatch R et al. introduced the benefits of the third frequency signal on cycle slip correction [13]. Liu et al. selected three linearly independent geometry-free pseudorange minus phase combination to determine the cycle slips on the original triple-frequency carrier phase observations [14]. de Lacy et al. defined five geometry-free linear combinations used in three steps for real-time cycle slip detection and repair on triple-frequency GNSS data [15]. Huang et al. defined two geometry-free phase combinations and one geometry-free pseudorange minus phase linear combination to detect and correct cycle slip and applied an effective decorrelation search based on LAMBDA and least squares minimum principle to calculate and determine the cycle slips [16]. Zhao et al. used three combinations, namely extra-wide lane, wide lane, and narrow lane, to determine cycle slips sequentially in three cascaded steps and results showed that this method performed well under high ionospheric activity [17]. Zeng et al. used triple-frequency combinations to detect and repair cycle slip under ionospheric disturbance with BDS data [18].

A real-time quadruple-frequency cycle slip detection and repair algorithm based on the four chosen linear combinations is proposed in the paper. When the four detection combinations are determined, cycle slips on the original carrier phase observations can be uniquely determined. The following section describes the choices of the first, the second, the third and the fourth detection combinations in detail and introduces the method of recovering cycle slip on each frequency based on the chosen four combinations. Then, the BDS and Galileo quadruple-frequency static and kinematic data with simulated cycle slips are used to test the performance of the proposed algorithm. Finally, conclusions are drawn.

II. PROPOSED METHOD

The pseudorange and carrier observation equations can be expressed as:

$$\rho_i = r + c(dt_u - dt^s) + T + \gamma_i I_1 + \varepsilon_{\rho_i} \quad (1)$$

$$\phi_i = \lambda_i \varphi_i = r + c(dt_u - dt^s) + T - \gamma_i I_1 + \lambda_i N_i + \varepsilon_{\phi_i} \quad (2)$$

where $i = 1, 2, 3, 4$ indicates the four frequencies. For BDS, the signal frequencies f_1, f_2, f_3, f_4 are 1561.098 MHz, 1575.42 MHz, 1176.45 MHz and 1268.52 MHz corresponding to B1I, B1C, B2a and B3I, respectively. For Galileo, the signal frequencies on f_1, f_2, f_3, f_4 are 1575.42 MHz, 1176.45 MHz, 1207.14 MHz and 1278.75 MHz, corresponding to E1, E5a, E5b and E6, respectively. ρ_i and ϕ_i are pseudorange and carrier phase observations on frequency f_i in meters. φ_i is carrier phase observation on frequency f_i in cycles and λ_i is corresponding wavelength. r is geometric distance. dt_u and dt^s are receiver clock error and satellite clock error in second. c is light speed. T is the tropospheric delay. I_1 is the first-order ionospheric group delay on the frequency f_1 and γ_i is ionospheric delay coefficient of f_i which is $\gamma_i = f_1^2/f_i^2$. N_i is integer ambiguity of f_i and the difference of N_i between two continuous epochs which can be expressed as ΔN_i is cycle slip on frequency f_i . ε_{ρ_i} and ε_{ϕ_i} are pseudorange observation noise and carrier phase observation noise in meters on frequency f_i and are assumed the same on four frequencies. On the basis of the original quadruple-frequency observations, the linear combinations of carrier phase observations and pseudorange observations in meters can be defined as follows:

$$\phi_{ijkt} = \frac{if_1\phi_1 + jf_2\phi_2 + kf_3\phi_3 + tf_4\phi_4}{if_1 + jf_2 + kf_3 + tf_4} \quad (3)$$

$$\rho_{abcd} = a\rho_1 + b\rho_2 + c\rho_3 + d\rho_4 \quad (4)$$

where ϕ_{ijkt} and ρ_{abcd} are the combined carrier phase and pseudorange in meters, (i, j, k, t) is the coefficient of carrier phase observations, and (a, b, c, d) is the coefficient of pseudorange observations. For carrier phase combination, the linearly combined frequency, wavelength, integer ambiguity and ionospheric delay are given by:

$$f_{ijkt} = if_1 + jf_2 + kf_3 + tf_4 \quad (5)$$

$$\lambda_{ijkt} = \frac{c}{if_1 + jf_2 + kf_3 + tf_4} \quad (6)$$

$$N_{ijkt} = iN_1 + jN_2 + kN_3 + tN_4 \quad (7)$$

$$I_{ijkt} = -\frac{\lambda_{ijkt}}{\lambda_1} \left(i + j\frac{f_1}{f_2} + k\frac{f_1}{f_3} + t\frac{f_1}{f_4} \right) I_1 \quad (8)$$

For pseudorange combination, the linearly combined ionospheric delay is given by:

$$I_{abcd} = \left(a + b\frac{f_1^2}{f_2^3} + c\frac{f_1^2}{f_3^3} + d\frac{f_1^2}{f_4^3} \right) I_1 \quad (9)$$

When the coefficients of carrier phase observations (i, j, k, t) are integers, combined ambiguity N_{ijkt} can maintain integer and the combined cycle slip ΔN_{ijkt} can be calculated by term (7) when cycle slips on four frequencies which are expressed by $\Delta N_1, \Delta N_2, \Delta N_3$ and ΔN_4 occur

A. FIRST DETECTION COMBINATION

The geometry-free and ionospheric-free (GFIF) pseudorange/carrier linear combination in cycles is used as the first detection combination which can be expressed as

follow (10), as shown at the bottom of this page. where (i, j, k, t) is the coefficient of carrier phase observations and (a, b, c, d) is the coefficient of pseudorange observations. The combination should satisfy two constraints below for eliminating geometry and ionosphere:

$$a + b + c + d = 1 \tag{11}$$

$$a + b \frac{f_1^2}{f_2^3} + c \frac{f_1^2}{f_3^3} + d \frac{f_1^2}{f_4^3} = -\frac{\lambda_{ijkt}}{\lambda_1} \left(i + j \frac{f_1}{f_2} + k \frac{f_1}{f_3} + t \frac{f_1}{f_4} \right) \tag{12}$$

Assuming that the pseudorange observation noise and carrier phase observation noise are white Gaussian noise (WGN), the variance of L_1 in cycles can be expressed as follows in accordance with the variance covariance propagation law:

$$\sigma_{L_1}^2 = \frac{(i^2 f_1^2 + j^2 f_2^2 + k^2 f_3^2 + t^2 f_4^2)}{c^2} \sigma_\phi^2 + \frac{a^2 + b^2 + c^2 + d^2}{\lambda_{ijkt}^2} \sigma_\rho^2 \tag{13}$$

where σ_ρ and σ_ϕ are pseudorange and carrier phase noise standard deviation in meters. The difference of L_1 between continuous epochs which is expressed as ΔL_1 satisfies Gaussian distribution and the average is ΔN_{ijkt} and the variance is $2\sigma_{L_1}^2$. It can be expressed as follows:

$$\Delta L_1 \sim N \left(\Delta N_{ijkt}, 2\sigma_{L_1}^2 \right) \tag{14}$$

where $N(\mu, \sigma^2)$ expresses Gaussian distribution, μ is average and σ^2 is variance. The threshold is set as 0.5 cycles so that the cycle slips can be fixed to the integer by rounding off the float estimation. The probability of successfully determining cycle slip defined as fixing probability in this research is expressed as follows:

$$P(|\Delta L_1 - \Delta N_{ijkt}| < 0.5) = 2\Phi \left(\frac{0.5}{\sqrt{2\sigma_{L_1}^2}} \right) - 1 \tag{15}$$

where

$$\Phi(x) = P(X \leq x) = \frac{1}{2} \left[1 + \operatorname{erf} \left(\frac{x}{\sqrt{2}} \right) \right] \tag{16}$$

and

$$\operatorname{erf}(x) = \frac{2}{\sqrt{\pi}} \int_0^x e^{-t^2} dt \tag{17}$$

The optimal coefficient of pseudorange observation (a, b, c, d) can be determined by the below term when the coefficient of carrier phase observations (i, j, k, t) is given (18), as shown at the bottom of this page, where $\min\{\bullet\}$ expresses the minimum value. We can use the Lagrange Multiplier Method to solve the term of (18). We construct the function as follows:

$$\begin{aligned} \text{Lag} &= \frac{(i^2 f_1^2 + j^2 f_2^2 + k^2 f_3^2 + t^2 f_4^2)}{c^2} \sigma_\phi^2 \\ &+ \frac{a^2 + b^2 + c^2 + d^2}{\lambda_{i,j,k,t}^2} \sigma_\rho^2 \\ &+ \alpha (a + b + c + d - 1) + \beta \\ &\times \left(a + b \frac{f_1^2}{f_2^3} + c \frac{f_1^2}{f_3^3} + d \frac{f_1^2}{f_4^3} + \frac{\lambda_{i,j,k,t}}{\lambda_1} \left(i + j \frac{f_1}{f_2} + k \frac{f_1}{f_3} + t \frac{f_1}{f_4} \right) \right) \end{aligned} \tag{19}$$

Then the optimal solution is as follows:

$$\begin{pmatrix} a \\ b \\ c \\ d \\ \alpha \\ \beta \end{pmatrix} = \begin{pmatrix} 1 & 1 & 1 & 1 & 0 & 0 \\ 1 & \frac{f_1^2}{f_2^3} & \frac{f_1^2}{f_3^3} & \frac{f_1^2}{f_4^3} & 0 & 0 \\ \frac{2\sigma_\rho^2}{\lambda_{ijkt}^2} & 0 & 0 & 0 & 1 & 1 \\ 0 & \frac{2\sigma_\rho^2}{\lambda_{ijkt}^2} & 0 & 0 & 1 & \frac{f_1^2}{f_2^3} \\ 0 & 0 & \frac{2\sigma_\rho^2}{\lambda_{ijkt}^2} & 0 & 1 & \frac{f_1^2}{f_3^3} \\ 0 & 0 & 0 & \frac{2\sigma_\rho^2}{\lambda_{ijkt}^2} & 1 & \frac{f_1^2}{f_4^3} \end{pmatrix}^{-1} \times \begin{pmatrix} 1 \\ -\frac{\lambda_{ijkt}}{\lambda_1} \left(i + j \frac{f_1}{f_2} + k \frac{f_1}{f_3} + t \frac{f_1}{f_4} \right) \\ 0 \\ 0 \\ 0 \\ 0 \end{pmatrix} \tag{20}$$

$$\begin{aligned} L_1 &= \frac{\phi_{ijkt} - \rho_{abcd}}{\lambda_{ijkt}} = \frac{\lambda_{ijkt} (if_1\phi_1 + jf_2\phi_2 + kf_3\phi_3 + tf_4\phi_4) - (a\rho_1 + b\rho_2 + c\rho_3 + d\rho_4)}{\lambda_{ijkt}} \\ &= \frac{if_1\phi_1 + jf_2\phi_2 + kf_3\phi_3 + tf_4\phi_4}{c} - \frac{a\rho_1 + b\rho_2 + c\rho_3 + d\rho_4}{\lambda_{ijkt}} \end{aligned} \tag{10}$$

$$\min \left\{ \begin{aligned} &\frac{(i^2 f_1^2 + j^2 f_2^2 + k^2 f_3^2 + t^2 f_4^2)}{c^2} \sigma_\phi^2 + \frac{a^2 + b^2 + c^2 + d^2}{\lambda_{i,j,k,t}^2} \sigma_\rho^2 | a + b + c + d = 1, \\ &a + b \frac{f_1^2}{f_2^3} + c \frac{f_1^2}{f_3^3} + d \frac{f_1^2}{f_4^3} = -\frac{\lambda_{i,j,k,t}}{\lambda_1} \left(i + j \frac{f_1}{f_2} + k \frac{f_1}{f_3} + t \frac{f_1}{f_4} \right) \end{aligned} \right\} \tag{18}$$

TABLE 1. Best pseudorange/carrier phase combinations.

(i, j, k, t)	(a, b, c, d)	λ_{ijkl} (meters)	$\sqrt{2\sigma_{L_1}^2}$ (cycles)	Fixing probability
BDS				
(-1 1 0 0)	(0.47651, 0.48955, -0.07180, 0.10573)	20.93	0.0344	1.0000
Galileo				
(0 -1 1 0)	(-0.07555, 0.43727, 0.37907, 0.25920)	9.77	0.0366	1.0000

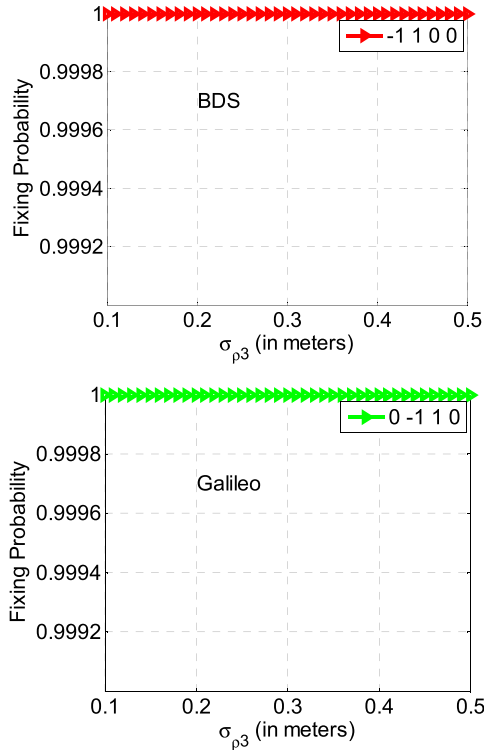


FIGURE 1. Fixing probability of BDS (top) and Galileo (bottom) varying with pseudorange standard deviation (The first detection combination).

As the term (20) shows, the optimal solution of (a, b, c, d) is related to σ_ρ^2 and (i, j, k, t) . As the term (13) shows, the combined noise is related to carrier phase coefficients (i, j, k, t) , and in order to reduce the combined noise, carrier phase coefficients (i, j, k, t) can not be too large. As a result, the range of (i, j, k, t) varies from -5 to $+5$ in this research. Table 1 lists the best pseudorange/carrier phase combinations for BDS and Galileo according to the fixing probability calculated by the term of (15) when $\sigma_\rho = 0.3\text{m}$, $\sigma_\phi = 0.003\text{m}$. Fig 1 shows the results of fixing probability varying with pseudorange standard deviation when the carrier phase standard is set as 0.003 m . As Fig. 1 shows, the fixing probabilities of $(-1\ 1\ 0\ 0)$ for BDS and $(0\ -1\ 1\ 0)$ for Galileo are almost 100% even when σ_ρ is 0.5 m . As a result, we choose $(-1\ 1\ 0\ 0)$ for BDS and $(0\ -1\ 1\ 0)$ for Galileo as the first carrier phase combination.

B. SECOND DETECTION COMBINATION

When the combined cycle slip of the first carrier phase combination is fixed and repaired, the first carrier phase

combination is used to provide geometrical reference for the second carrier phase combination. The second detection combination in cycles can be expressed as follows:

$$L_2 = \frac{\lambda_{ijkl} \frac{(if_1\phi_1 + jf_2\phi_2 + kf_3\phi_3 + tf_4\phi_4)}{c} - \lambda_{pquv} \frac{(pf_1\phi_1 + qf_2\phi_2 + uf_3\phi_3 + vf_4\phi_4)}{c}}{\lambda_{pquv}} \tag{21}$$

where (i, j, k, t) is the coefficient of the first carrier phase combination, i.e. $(-1\ 1\ 0\ 0)$ for BDS and $(0\ -1\ 1\ 0)$ for Galileo, (p, q, u, v) is the coefficient of the second carrier phase combination. The second detection combination eliminates the geometry but the ionospheric delay still exists and the value of ionospheric delay in cycles is as follows (22), as shown at the bottom of the next page. In accordance with the variance-covariance propagation law, the variance of L_2 in cycles can be expressed as follows (23), as shown at the bottom of the next page. The difference of L_2 between continuous epochs which is expressed as ΔL_2 satisfies Gaussian distribution and the average is $\Delta N_{pquv} + \Delta I_{L_2}$ and variance is $2\sigma_{L_2}^2$. It can be expressed as follows:

$$\Delta L_2 \sim N \left(\Delta N_{pquv} + \Delta I_{L_2}, 2\sigma_{L_2}^2 \right) \tag{24}$$

The fixing probability can be expressed as follows:

$$P(|\Delta L_2 - \Delta N_{pquv}| < 0.5) = \Phi \left(\frac{0.5 - \Delta I_{L_2}}{\sqrt{2\sigma_{L_2}^2}} \right) - \Phi \left(\frac{-0.5 - \Delta I_{L_2}}{\sqrt{2\sigma_{L_2}^2}} \right) \tag{25}$$

The fixing probability is related to $|\Delta I_{L_2}|$ and $\sigma_{L_2}^2$. The range of (p, q, u, v) varies from -5 to $+5$ in this research. For each choice of (p, q, u, v) , we can calculate the fixing probability according to the term of (25). The larger the fixing probability is, the better the choice is. Liu et al. showed that in the equatorial region such as Hong Kong, the ionospheric slant total electron content rate (TECR) was about 0.01 TECU/s during quiet ionosphere periods and it rose to 0.03 TECU/s during disturbed ionosphere period [19]. We set the TECR as 0.03 TECU/s to assess the validity of different carrier phase combinations under high ionospheric activity. Table 2 lists the ten best carrier phase combinations for BDS and Galileo according to the fixing probability calculated by the term of (25) and the carrier phase standard deviation is set as 0.003 m . Fig. 2 shows the fixing probability varying with TECR. As Fig. 2 shows, the fixing probabilities of

TABLE 2. Ten best carrier phase combinations.

(p, q, u, v)	λ_{pquv} (meters)	$ \Delta I_{L_2} $ (cycles)	$\sqrt{2\sigma_{L_2}^2}$ (cycles)	Fixing probability
BDS				
(-5 4 -3 4)	7.33	0.0532	0.1027	0.99999
(-4 3 -3 4)	11.27	0.0532	0.1027	0.99999
(-4 5 3 -4)	3.41	-0.0532	0.1027	0.99999
(-3 2 -3 4)	24.42	0.0532	0.1027	0.99999
(-3 4 3 -4)	4.07	-0.0532	0.1027	0.99999
(2 -1 3 -4)	146.53	-0.0532	0.1027	0.99999
(-2 3 3 -4)	5.05	-0.0532	0.1027	0.99999
(1 0 3 -4)	18.32	-0.0532	0.1027	0.99999
(-1 2 3 -4)	6.66	-0.0532	0.1027	0.99999
(0 1 3 -4)	9.77	-0.0532	0.1027	0.99999
Galileo				
(0 -5 4 1)	1.33	-0.0049	0.0713	0.99999
(0 -4 3 1)	1.54	-0.0049	0.0713	0.99999
(0 -4 5 -1)	5.86	0.0049	0.0713	0.99999
(0 -3 2 1)	1.83	-0.0049	0.0713	0.99999
(0 -3 4 -1)	14.65	0.0049	0.0713	0.99999
(0 -2 1 1)	2.25	-0.0049	0.0713	0.99999
(0 -1 0 1)	2.93	-0.0049	0.0713	0.99999
(0 0 -1 1)	4.19	-0.0049	0.0713	0.99999
(0 1 -2 1)	7.33	-0.0049	0.0713	0.99999
(0 2 -3 1)	29.31	-0.0049	0.0713	0.99999

those ten carrier phase combinations are larger than 99.99% for BDS and Galileo even when TECR is 0.03 TECU/s, so that they can determine cycle slips efficiently under high ionospheric activity. Due to their having the same fixing probability, we cannot determine the best combination during the second stage so that they are all set as alternative combinations and provide geometrical reference for the third carrier phase combination

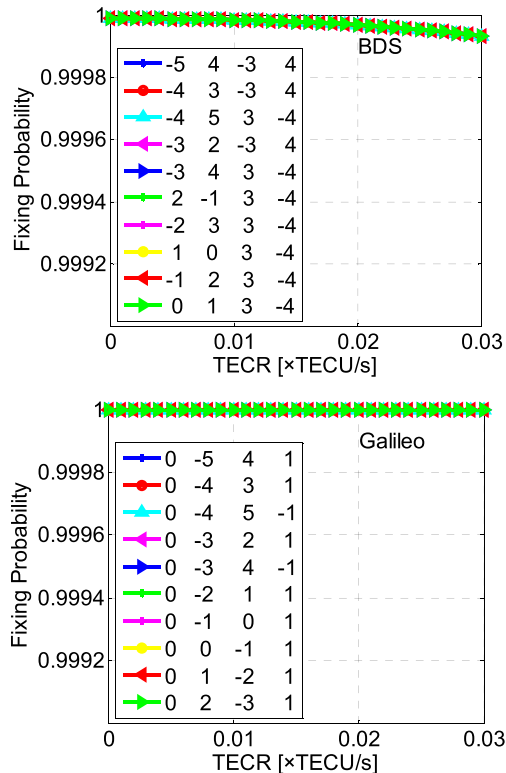


FIGURE 2. Fixing probability of BDS (top) and Galileo (bottom) varying with TECR (The second detection combination).

C. THIRD DETECTION COMBINATION

When the combined cycle slip of the second carrier phase combination is fixed and repaired, the second carrier phase combination is used to provide geometrical reference for the third carrier phase combination.

The third detection combination in cycles can be expressed as follows (26), as shown at the bottom of this page, where

$$I_{L_2} = \frac{\left\{ \lambda_{ijkt} \left(i + j \frac{f_1}{f_2} + k \frac{f_1}{f_3} + t \frac{f_1}{f_4} \right) - \lambda_{pquv} \left(p + q \frac{f_1}{f_2} + u \frac{f_1}{f_3} + v \frac{f_1}{f_4} \right) \right\} \frac{I_1}{\lambda_1}}{\lambda_{pquv}} \tag{22}$$

$$\sigma_{L_2}^2 = \frac{\left\{ \left(\frac{\lambda_{ijkt} i - \lambda_{pquv} p}{c} f_1 \right)^2 + \left(\frac{\lambda_{ijkt} j - \lambda_{pquv} q}{c} f_2 \right)^2 + \left(\frac{\lambda_{ijkt} k - \lambda_{pquv} u}{c} f_3 \right)^2 + \left(\frac{\lambda_{ijkt} t - \lambda_{pquv} v}{c} f_4 \right)^2 \right\} \sigma_\phi^2}{\lambda_{pquv}^2} \tag{23}$$

$$L_3 = \frac{\lambda_{pquv} \frac{(pf_1\phi_1 + qf_2\phi_2 + uf_3\phi_3 + vf_4\phi_4)}{c} - \lambda_{wxyz} \frac{(wf_1\phi_1 + xf_2\phi_2 + yf_3\phi_3 + zf_4\phi_4)}{c}}{\lambda_{wxyz}} \tag{26}$$

$$I_{L_3} = \frac{\left\{ \lambda_{pquv} \left(p + q \frac{f_1}{f_2} + u \frac{f_1}{f_3} + v \frac{f_1}{f_4} \right) - \lambda_{wxyz} \left(w + x \frac{f_1}{f_2} + y \frac{f_1}{f_3} + z \frac{f_1}{f_4} \right) \right\} \frac{I_1}{\lambda_1}}{\lambda_{wxyz}} \tag{27}$$

$$\sigma_{L_3}^2 = \frac{\left\{ \left(\frac{\lambda_{pquv} p - \lambda_{wxyz} w}{c} f_1 \right)^2 + \left(\frac{\lambda_{pquv} q - \lambda_{wxyz} x}{c} f_2 \right)^2 + \left(\frac{\lambda_{pquv} u - \lambda_{wxyz} y}{c} f_3 \right)^2 + \left(\frac{\lambda_{pquv} v - \lambda_{wxyz} z}{c} f_4 \right)^2 \right\} \sigma_\phi^2}{\lambda_{wxyz}^2} \tag{28}$$

(p, q, u, v) is the coefficient of the second alternative carrier phase combination listed in Table 2 and (w, x, y, z) is the coefficient of the third carrier phase combination. The third combination eliminates the geometry but the ionospheric delay still exists and the value of ionospheric delay in cycles is as follows (27), as shown at the bottom of the previous page. The variance of L_3 in cycles can be expressed as follows in accordance with the variance-covariance propagation law (28), as shown at the bottom of the previous page.

The first-order time difference of L_3 between continuous epochs which is expressed as ΔL_3 satisfies Gaussian distribution and the average is $\Delta N_{wxyz} + \Delta I_{L_3}$ and variance is $2\sigma_{L_3}^2$. It can be expressed as follows:

$$\Delta L_3 \sim N(\Delta N_{wxyz} + \Delta I_{L_3}, 2\sigma_{L_3}^2) \quad (29)$$

The fixing probability can be expressed as follows:

$$P(|\Delta L_3 - \Delta N_{wxyz}| < 0.5) = \Phi\left(\frac{0.5 - \Delta I_{L_3}}{\sqrt{2\sigma_{L_3}^2}}\right) - \Phi\left(\frac{-0.5 - \Delta I_{L_3}}{\sqrt{2\sigma_{L_3}^2}}\right) \quad (30)$$

Assuming that cycle slip occurs at epoch k and there are no cycle slips or cycle slips have been repaired at epoch $k-1$ and $k-2$, the second-order time difference of L_3 between continuous three epochs which is expressed as $\Delta\Delta L_3$ satisfies Gaussian distribution and the mean value is ΔN_{wxyz} and the variance is $4\sigma_{L_3}^2$. It can be expressed as follows:

$$\Delta\Delta L_3 \sim N(\Delta N_{wxyz}, 4\sigma_{L_3}^2) \quad (31)$$

The fixing probability can be expressed as follows:

$$P(|\Delta\Delta L_3 - \Delta N_{wxyz}| < 0.5) = 2\Phi\left(\frac{0.5}{\sqrt{4\sigma_{L_3}^2}}\right) - 1 \quad (32)$$

The range of (w, x, y, z) varies from -5 to $+5$ in this research. Table 3 and Table 4 list the best carrier phase combinations of the first-order and the second-order time-difference methods for BDS and Galileo according to the fixing probability calculated by the term of (30) and (32) when the TECR is set as 0.03 TECU/s and the carrier phase standard deviation is set as 0.003 m. For BDS, the fixing probability of the second-order time-difference method, i.e. 0.99999, is larger than that of the first-order time-difference method, i.e. 0.98900, so that we use the second-order time-difference method to detect and repair the combined cycle slips on the third detection combination. For Galileo, the fixing probability of the first-order time-difference method, i.e. 0.99999, is larger than that of the second-order time-difference method, i.e. 0.99997, so that we use the first-order time-difference method to detect and repair the combined cycle slips on the third detection combination. Fig.3 shows the fixing probability of the second-order time-difference method for BDS

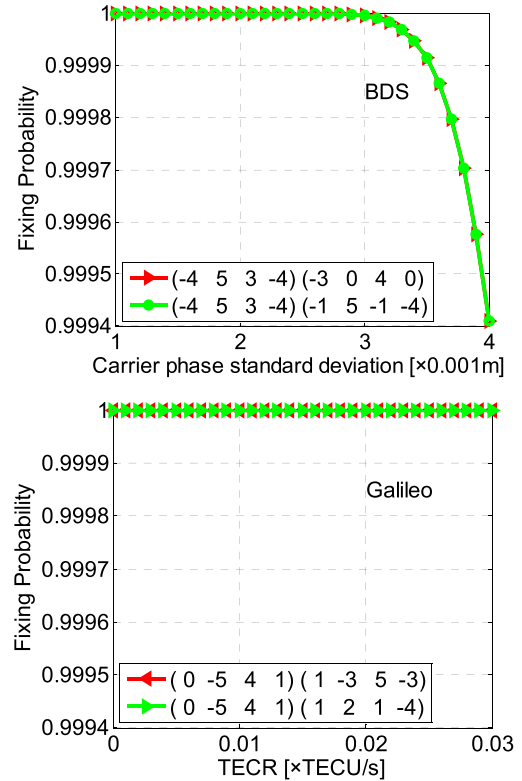


FIGURE 3. Fixing probability of the second-order time-difference method for BDS varying with carrier phase observation noise (top) and the first-order time-difference method for Galileo varying with TECR (bottom) (The third detection combination).

varying with carrier phase observation noise and the first-order time-difference method for Galileo varying with TECR. As Fig.3 shows, for BDS, the fixing probability decreases when carrier phase standard deviation grows, but the fixing probability is still larger than 99.94% even when the carrier phase standard deviation is 0.004 m. For Galileo, the fixing probability is almost 100% even when TECR is 0.03 TECU/s so that it can detect and repair cycle slip efficiently under high ionospheric activity. Until now, the second carrier phase combination is determined as listed in Table 3 and Table 4. In accordance to the fixing probability of the third detection combination, there are two equal choices for the third carrier phase combination for both BDS and Galileo, i.e. $(-3 \ 0 \ 4 \ 0)$ and $(-1 \ 5 \ -1 \ -4)$ for BDS and $(1 \ -3 \ 5 \ -3)$ and $(1 \ 2 \ 1 \ -4)$ for Galileo, and they are all set as alternative combinations to provide geometrical reference for the fourth carrier phase combination.

D. FOURTH DETECTION COMBINATION

When the combined cycle slip of the third carrier phase combination is fixed and repaired, the third carrier phase combination is used to provide geometrical reference for the fourth carrier phase combination. The fourth detection combination in cycles can be expressed as follows (33), as shown at the bottom of the next page, where (w, x, y, z) is the coefficient of the third carrier phase combination listed in Table 3 and

TABLE 3. Best carrier phase combinations of the first-order time-difference method.

(p, q, u, v)	(w, x, y, z)	$ \Delta I_{L_3} $ (cycles)	$\sqrt{2\sigma_{L_3}^2}$ (cycles)	Fixing probability
BDS				
(-5 4 -3 4)	(3 -4 -4 5)	0.0586	0.1882	0.98900
Galileo				
(0 -5 4 1)	(1 -3 5 -3)	-0.0595	0.0881	0.99999
(0 -5 4 1)	(1 2 1 -4)	-0.0595	0.0881	0.99999

TABLE 4. Best carrier phase combinations of the second-order time-difference method.

(p, q, u, v)	(w, x, y, z)	$\sqrt{4\sigma_{L_3}^2}$ (cycles)	Fixing probability
BDS			
(-4 5 3 -4)	(-3 0 4 0)	0.1091	0.99999
(-4 5 3 -4)	(-1 5 -1 -4)	0.1091	0.99999
Galileo			
(0 -2 1 1)	(-3 -4 5 3)	0.1203	0.99997
(0 -2 1 1)	(-3 -2 4 2)	0.1203	0.99997
(0 -2 1 1)	(-3 0 3 1)	0.1203	0.99997
(0 -2 1 1)	(-3 2 2 0)	0.1203	0.99997
(0 -2 1 1)	(3 -4 -1 1)	0.1203	0.99997

Table 4, and (l, m, n, g) is the coefficient of the fourth carrier phase combination. The fourth detection combination eliminates the geometry but the ionospheric delay still exists and the value of ionospheric delay is as follows (35), as shown at the bottom of this page, In accordance with the variance-covariance propagation law, the variance of L_4 in cycles can be expressed as follows (34), as shown at the bottom of this page, The first-order time difference of L_4 between continuous epochs which is expressed as ΔL_4 satisfies Gaussian distribution and the average is $\Delta N_{lmng} + \Delta I_{L_4}$ and the variance is $2\sigma_{L_4}^2$. It can be expressed as follows:

$$\Delta L_4 \sim N(\Delta N_{lmng} + \Delta I_{L_4}, 2\sigma_{L_4}^2) \quad (36)$$

TABLE 5. Best carrier phase combinations of the first-order time-difference method.

(w, x, y, z)	(l, m, n, g)	$ \Delta I_{L_4} $ (cycles)	$\sqrt{2\sigma_{L_4}^2}$ (cycles)	Fixing probability
BDS				
(-1 5 -1 -4)	(3 0 -5 1)	-0.0266	0.1878	0.99163
Galileo				
(1 2 1 -4)	(3 2 -4 -2)	0.9026	1.3187	0.23632

The fixing probability can be expressed as follows:

$$P(|\Delta L_4 - \Delta N_{lmng}| < 0.5) = \Phi\left(\frac{0.5 - \Delta I_{L_4}}{\sqrt{2\sigma_{L_4}^2}}\right) - \Phi\left(\frac{-0.5 - \Delta I_{L_4}}{\sqrt{2\sigma_{L_4}^2}}\right) \quad (37)$$

Be same with the third detection combination, the second-order time difference of L_4 between continuous three epochs which is expressed as $\Delta\Delta L_4$ satisfies Gaussian distribution and the mean value is ΔN_{lmng} and the variance is $4\sigma_{L_4}^2$. It can be expressed as follows:

$$\Delta\Delta L_4 \sim N(\Delta N_{lmng}, 4\sigma_{L_4}^2) \quad (38)$$

The fixing probability can be expressed as follows:

$$P(|\Delta\Delta L_4 - \Delta N_{lmng}| < 0.5) = 2\Phi\left(\frac{0.5}{\sqrt{4\sigma_{L_4}^2}}\right) - 1 \quad (39)$$

The range of (l, m, n, g) varies from -5 to $+5$ in this research. Table 5 and Table 6 list the best carrier phase combinations of the first-order and the second-order time-difference methods for BDS and Galileo according to the fixing probability calculated by the term of (37) and (39) when the TECR is set as 0.03 TECU/s and the carrier phase standard deviation is set as 0.003 m. For BDS, the fixing probability of the first-order time difference method, i.e. 0.99163, is larger than that of the second-order time difference method, i.e. 0.94235, so that we use the first-order time-difference method

$$L_4 = \frac{\lambda_{wxyz} \frac{(wf_1\phi_1 + xf_2\phi_2 + yf_3\phi_3 + zf_4\phi_4)}{c} - \lambda_{lmng} \frac{(lf_1\phi_1 + mf_2\phi_2 + nf_3\phi_3 + gf_4\phi_4)}{c}}{\lambda_{lmng}} \quad (33)$$

$$I_{L_4} = \frac{\left\{ \lambda_{wxyz} \left(w + x\frac{f_1}{f_2} + y\frac{f_1}{f_3} + z\frac{f_1}{f_4} \right) - \lambda_{lmng} \left(l + m\frac{f_1}{f_2} + n\frac{f_1}{f_3} + g\frac{f_1}{f_4} \right) \right\} \frac{l_1}{\lambda_1}}{\lambda_{lmng}} \quad (34)$$

$$\sigma_{L_4}^2 = \frac{\left\{ \left(\frac{\lambda_{wxyz}w - \lambda_{lmng}l}{c} f_1 \right)^2 + \left(\frac{\lambda_{wxyz}x - \lambda_{lmng}m}{c} f_2 \right)^2 + \left(\frac{\lambda_{wxyz}y - \lambda_{lmng}n}{c} f_3 \right)^2 + \left(\frac{\lambda_{wxyz}z - \lambda_{lmng}g}{c} f_4 \right)^2 \right\} \sigma_\phi^2}{\lambda_{lmng}^2} \quad (35)$$

TABLE 6. Best carrier phase combinations of the second-order time-difference method.

(w, x, y, z)	(l, m, n, g)	$\sqrt{4\sigma_{L_4}^2}$ (cycles)	Fixing probability
BDS			
(-1 5 -1 -4)	(-4 2 2 -2)	0.2634	0.94235
(-1 5 -1 -4)	(-4 3 -3 -1)	0.2634	0.94235
Galileo			
(1 -3 5 -3)	(-3 2 2 0)	0.1200	0.99997
(1 -3 5 -3)	(4 -5 3 -3)	0.1200	0.99997

to detect and repair the combined cycle slips on the fourth detection combination. For Galileo, the fixing probability of the second-order time-difference method, i.e. 0.99997, is larger than that of the first-order time difference method, i.e. 0.23632, so that we use the second-order time-difference method to detect and repair the combined cycle slips on the fourth detection combination. Fig. 4 shows the fixing probability of the first-order time-difference method for BDS varying with TECR and the second-order time-difference method for Galileo varying with carrier phase observation noise. As Fig. 4 shows, for BDS, the fixing probability is larger than 99.16% when TECR is 0.03 TECU/s. For Galileo, the fixing probability is larger than 99.8% when the carrier phase standard deviation is 0.004 m. Until now, the third and the fourth carrier phase combinations for BDS and Galileo are determined as listed in Table 5 and Table 6. For BDS, the third carrier phase combination is (-1 5 -1 -4) and the fourth carrier phase combination is (3 0 -5 1), respectively. For Galileo, the third carrier phase combination is (1 -3 5 -3) and the fourth carrier phase combination is (-3 2 2 0) or (4 -5 3 -3). We select (-3 2 2 0) as the fourth carrier phase combination in this research. Actually, as Table 5 and 6 show, when we determinate the optimal combination, all factors affecting the fixing probability, including ionospheric delay and combined noise, are in units of cycles. Although the wavelength and the combined noise of (-3 2 2 0) and (4 -5 3 -3) are different in meters, their combined noise in cycles are same so that their fixing probabilities are the same. As a result, we can select (4 -5 3 -3) also as the fourth carrier phase combination in this research, too. To be brief, we choose (-3 2 2 0) as the fourth combination.

E. RECOVER CYCLE SLIPS ON EACH FREQUENCY

When the first, the second, the third and the fourth detection results are determined, the detection equation for BDS can be expressed as follows:

$$\begin{pmatrix} -1 & 1 & 0 & 0 \\ -4 & 5 & 3 & -4 \\ -1 & 5 & -1 & -4 \\ 3 & 0 & -5 & 1 \end{pmatrix} \begin{pmatrix} \Delta N_1 \\ \Delta N_2 \\ \Delta N_3 \\ \Delta N_4 \end{pmatrix} = \begin{pmatrix} int(\Delta L_1) \\ int(\Delta L_2) \\ int(\Delta L_3) \\ int(\Delta L_4) \end{pmatrix} \quad (40)$$

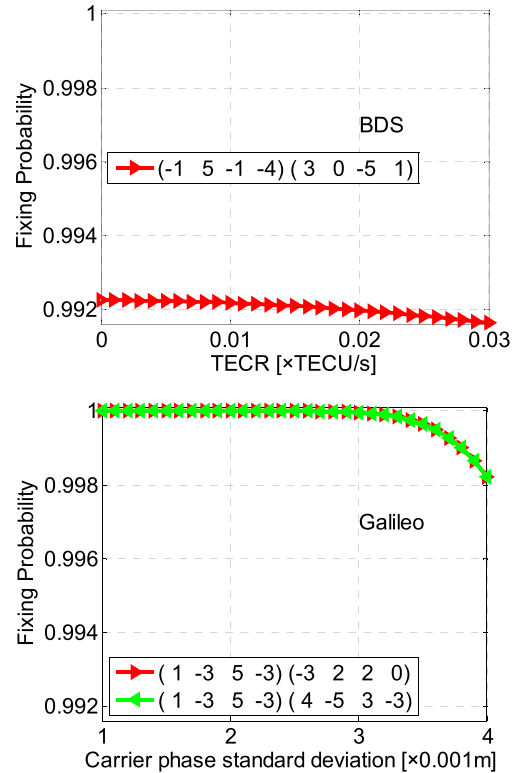


FIGURE 4. Fixing probability of the first-order time-difference method for BDS varying with TECR (top) and the second-order time-difference method for Galileo varying with carrier phase observation noise (bottom) (The fourth detection combination).

and the detection equation for Galileo can be expressed as follows:

$$\begin{pmatrix} 0 & -1 & 1 & 0 \\ 0 & -5 & 4 & 1 \\ 1 & -3 & 5 & -3 \\ -3 & 2 & 2 & 0 \end{pmatrix} \begin{pmatrix} \Delta N_1 \\ \Delta N_2 \\ \Delta N_3 \\ \Delta N_4 \end{pmatrix} = \begin{pmatrix} int(\Delta L_1) \\ int(\Delta L_2) \\ int(\Delta L_3) \\ int(\Delta L_4) \end{pmatrix} \quad (41)$$

where $(\Delta N_1, \Delta N_2, \Delta N_3, \Delta N_4)$ are cycle slips on f_1, f_2, f_3, f_4 , respectively. $int(x)$ means that x is rounded to the nearest integer. All coefficients in the term of (40) and (41) are integers so that the integer nature of $(\Delta N_1, \Delta N_2, \Delta N_3, \Delta N_4)$ is maintained.

III. DATA ANALYSIS

The proposed algorithm is tested on real quadruple-frequency data collected at Changsha on April 7, 2019. The receiver type is TRIMBLE ALLOY 5.37 which can receive BDS-2 signals, i.e. B1I and B3I, BDS-3 new OS signals, i.e. B1C and B2a, and quadruple-frequency Galileo signals, i.e. E1, E5a, E5b and E6. The observation interval is 30 s. The elevation mask angle is set as 10 degrees. Two BDS satellites, i.e. C21 and C28, and two Galileo satellites, i.e. E07 and E19, are used to assess the performance of the proposed algorithm. The satellite C21 data refers to GPS time 9:24 to 13:23, with elevation angle varying from 10 degrees to 34 degrees. The satellite C28 data refers to GPS time 11:50 to 17:50, with

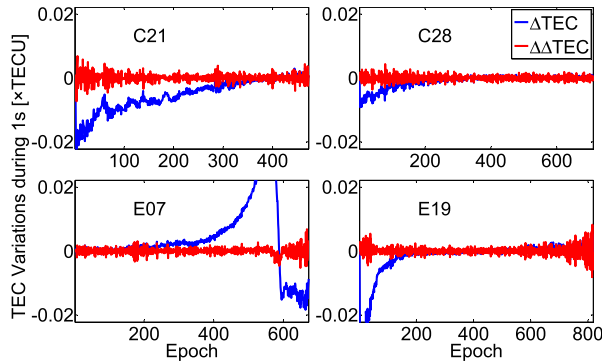


FIGURE 5. Ionospheric delay variations of C21 (top left), C28 (top right), E07 (bottom left) and E19 (bottom right). First-order time-difference TEC variations ΔTEC (blue) and second-order time-difference TEC variations $\Delta\Delta\text{TEC}$ (red).

elevation angle varying from 10 degrees to 87 degrees. The satellite E07 data refers to GPS time 00:00 to 05:40, with elevation angle varying from 10 degrees to 82 degrees. The satellite E19 data refers to GPS time 12:05 to 18:55, with elevation angle varying from 10 degrees to 69 degrees.

A. IONOSPHERIC ACTIVITY

Ionospheric delay variations are analyzed at first. The carrier phase observations of B1I and B3I for BDS and E1 and E6 for Galileo are used to calculate ionospheric delay variations. Fig. 5 shows the first-order and the second-order time-difference TEC variations of C21, C28, E07 and E19. As Fig. 5 shows, the first-order time-difference ionospheric delay variations (blue) for all involved satellites are significant. However, the trend component is not obvious in the second-order time-difference TEC variations (red) for all satellites involved. The second-order time-difference TEC variations are clustered around zero over the entire observation time. This indicates that the impact of ionospheric delay can be significantly reduced using the second-order time-difference method.

B. NOISE LEVEL OF COMBINATION

Fig. 6 shows the ΔL_1 , ΔL_2 , $\Delta\Delta L_3$ and ΔL_4 of C21 and C28 and the ΔL_1 , ΔL_2 , ΔL_3 and $\Delta\Delta L_4$ of E07 and E19. As Fig. 6 shows, the ionospheric delay variations in $\Delta\Delta L_3$ of C21 and C28 and $\Delta\Delta L_4$ of E07 and E19 have been eliminated and the detect results are lower than 0.5 cycles during the entire observation time for those four combinations. As a result, when the threshold is 0.5 cycles, the proposed algorithm can efficiently detect and repair cycle slips.

C. SIMULATED CYCLE SLIP TEST

In order to assess the performance of the proposed method, we simulated several cycle slip pairs on the original carrier phase observations. The small cycle slips range from 1 to 2 and they can occur on one, two, three or four frequencies simultaneously. At first, several random cycle slip pairs are simulated on the original carrier phase observations to test the

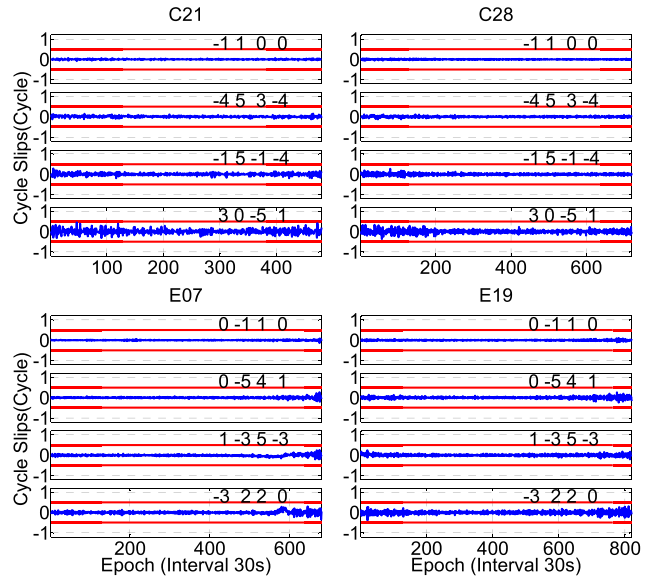


FIGURE 6. Detection results of the four combinations. Top left, top right, bottom left and bottom right are C21, C28, E07 and E19, respectively. The observation interval is 30 s.

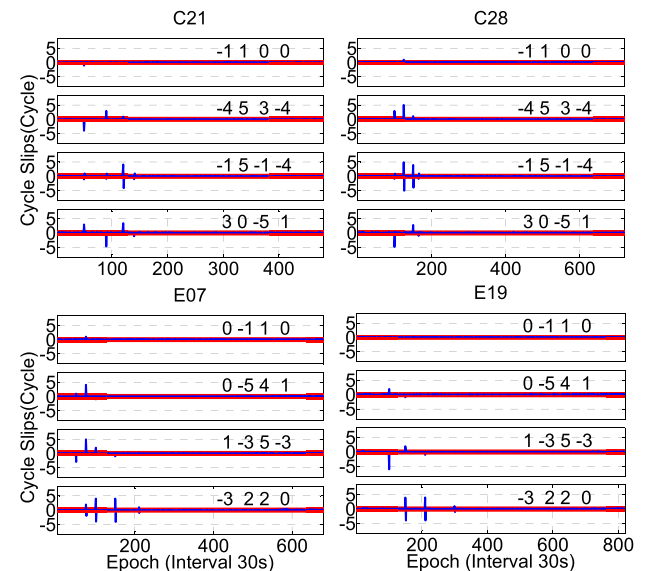


FIGURE 7. Detection results of the four combinations with simulated cycle slips. Top Left, Top Right, Bottom left and bottom right are C21, C28, E07 and E19, respectively. The observation interval is 30 s.

algorithm. Then, the particular cycle slip pairs are simulated to the observations every ten epochs to analyze the reliability and efficiency of the proposed method.

1) REPAIR RANDOM CYCLE SLIP PAIRS

We simulate two types of random cycle slips on the original carrier phase observations. The cycle slips include small and particular cycle slips. Fig.7 shows the random cycle slip detection results on the four combinations for each satellite. Table 7 lists all the detection results. As Fig.7 shows, the cycle slips, despite a small cycle size of 1, cause significant jump

TABLE 7. Cycle slip detection and repair results with simulated cycle slips.

PRN	Epoch	Simulated Cycle Slip	Cycle Slip Type	BDS				Estimated Cycle Slip
				ΔL_1	ΔL_2	$\Delta\Delta L_3$	ΔL_4	
				Galileo				
				ΔL_1	ΔL_2	ΔL_3	$\Delta\Delta L_4$	
BDS								
C21	50	(1 0 0 0)	Small	-0.97	-4.01	-0.91	2.88	(1 0 0 0)
C21	90	(0 0 1 0)	Small	0.11	3.03	-1.13	-5.20	(0 0 1 0)
C21	120	(1 1 0 0)	Particular	-0.03	0.99	4.16	2.94	(1 1 0 0)
C21	140	(1 1 1 1)	Particular	0.03	0.11	-1.13	-1.04	(1 1 1 1)
C28	100	(0 0 1 0)	Small	0.02	3.00	-1.01	-5.19	(0 0 1 0)
C28	125	(0 1 0 0)	Small	1.00	4.95	5.03	0.01	(0 1 0 0)
C28	150	(1 1 0 0)	Particular	0.02	0.99	4.03	2.96	(1 1 0 0)
C28	165	(1 1 1 1)	Particular	0.03	0.00	-1.03	-1.02	(1 1 1 1)
Galileo								
E07	50	(0 0 0 1)	Small	0.01	0.99	-3.00	0.04	(0 0 0 1)
E07	75	(0 0 1 0)	Small	0.99	4.01	4.99	1.95	(0 0 1 0)
E07	100	(0 1 1 0)	Particular	0.01	-1.03	2.01	4.01	(0 1 1 0)
E07	150	(0 1 1 1)	Particular	0.03	0.01	-0.97	4.08	(0 1 1 1)
E07	210	(1 1 1 1)	Particular	0.01	-0.01	0.03	1.01	(1 1 1 1)
E19	100	(0 0 0 2)	Small	0.02	1.97	-5.99	0.01	(0 0 0 2)
E19	150	(0 1 1 0)	Particular	0.01	-1.01	2.03	4.08	(0 1 1 0)
E19	210	(0 1 1 1)	Particular	-0.01	0.03	-1.05	4.01	(0 1 1 1)
E19	300	(1 1 1 1)	Particular	0.02	0.01	-0.03	1.04	(1 1 1 1)

on the four combinations. As to the particular cycle slip pairs, such as (1 1 0 0), (0 1 1 0), (0 1 1 1) and (1 1 1 1), these cycle slip pairs cannot be detected by the first or the second detection combination for BDS and Galileo, but they do not cause the discontinuity of these detection combinations so that these cycle slip pairs will not affect the above detection combinations providing geometrical reference for the subsequent detection combinations. In addition, they can be detected by the other detection combinations, such as the third or the fourth detection combination, so that those particular cycle slip pairs will be detected and repaired correctly, too. Table 7 summarizes all the detection results in the test. As listed, the proposed algorithm correctly detected and repaired all the random cycle slips.

2) REPAIR PARTICULAR CYCLE SLIP PAIRS

As discussed above, the particular cycle slip pairs with the form of (N, N, N, N), (N, N, 0, 0), (0, N, N, 0) and (0, N, N, N) cannot be detected by the first or the second detection combination of BDS and Galileo. We simulated those forms of cycle slip pairs to observations every ten epochs, which are (1 1 0 0) in C21, (1 1 1 1) in C28, (0 1 1 0) in E07, (0 1 1 1) in E07 and (1 1 1 1) in E19 on quadruple-frequency data, respectively. The repairing correct rates are 100% for all simulated cycle slips.

D. KINEMATIC TEST

In this section, BDS and Galileo data from the car-driven experiment are used to further evaluate the performance of the proposed algorithm under kinematic condition.



FIGURE 8. Observational environment and GNSS antenna in the car-driven experiment (trajectory of the car with yellow line).

The kinematic data are collected from the car-driven experiment conducted at Wuhan on April 17, 2019. The sampling interval is 0.05 s. The type of GNSS receiver is TRIMBLE ALLOY 5.37. Fig. 8 shows the observational environment and GNSS antenna in the car-driven experiment. BDS satellite C30 and Galileo satellite E26 are analyzed to verify the performance of the proposed algorithm. Fig. 9 shows the noise level of the four combinations. As Fig. 9 shows, the detect results are lower than 0.5 cycles during the entire observation time for those four combinations. Then, several simulated cycle slips are inserted to carrier phase observations. Fig. 10 and Table 8 show the detection results. Results show that the proposed algorithm is efficient when applied to kinematic application.

E. COMPARISONS WITH TRADITIONAL METHODS

Traditional methods to detect and repair cycle slip are mainly based on dual-frequency or triple-frequency

TABLE 8. Cycle slip detection and repair results with simulated cycle slips for C30 and E26.

PRN	Epoch	Simulated Cycle Slip	Cycle Slip Type	BDS				Estimated Cycle Slip
				ΔL_1	ΔL_2	$\Delta\Delta L_3$	ΔL_4	
				Galileo				
				ΔL_1	ΔL_2	ΔL_3	$\Delta\Delta L_4$	
BDS								
C30	1000	(0 0 1 0)	Small	0.01	3.13	-1.01	-5.14	(0 0 1 0)
C30	3200	(0 1 0 0)	Small	1.02	4.97	4.99	0.03	(0 1 0 0)
C30	4500	(1 1 0 0)	Particular	-0.01	1.01	4.02	2.99	(1 1 0 0)
C30	5050	(1 1 1 1)	Particular	0.02	0.01	-1.03	-1.07	(1 1 1 1)
Galileo								
E26	1000	(0 0 0 2)	Small	0.02	1.94	-6.01	0.01	(0 0 0 2)
E26	3150	(0 1 1 0)	Particular	0.01	-1.01	2.05	4.06	(0 1 1 0)
E26	6100	(0 1 1 1)	Particular	-0.01	0.03	-0.98	4.01	(0 1 1 1)
E26	7500	(1 1 1 1)	Particular	0.02	0.01	-0.03	1.03	(1 1 1 1)

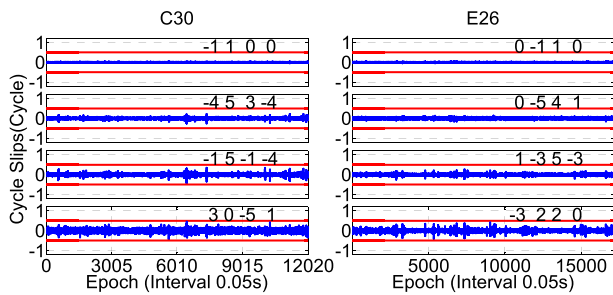


FIGURE 9. Detection results for C30 (left) and E26 (right) with sampling interval of 0.05 s.

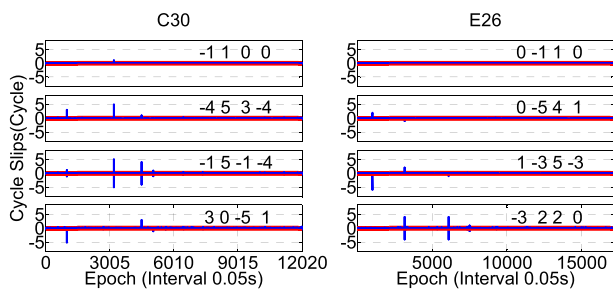


FIGURE 10. Detection results with simulated cycle slips for C30 (left) and E26 (right) with sampling interval of 0.05 s.

observations. Regarding the limitation of space, BDS satellite C21 observed at Changsha on April 7, 2019 is used as an example to assess the performance of the traditional dual-frequency and triple-frequency methods. The performance of the proposed method using this satellite’s data can be seen from Fig.6 and we do not show them again.

1) PERFORMANCE OF DUAL-FREQUENCY METHOD

We use B1I and B3I observations to assess the performance of dual-frequency method. TurboEdit method has been widely used to detect and repair dual-frequency cycle slip [9].

This method uses MW combination and GF (Geometry-Free) combination (some researches call this combination as ionospheric residual combination [10]) to detect and repair cycle slips. In order to detect and repair cycle slip of one cycle, the threshold of MW combination is set as 0.5 cycles. Assuming the carrier phase noise is 0.02 cycles on each frequency, according to the variance covariance propagation law, the threshold of GF combination is set as 0.0773 cycles. One point should be mentioned is that the detection threshold in TurboEdit method is adaptive according to reference [9]. It is reasonable from the static point. However, our ultimate goal is repairing cycle slips but not only detecting cycle slips. For MW combination, it maintains the integer nature of cycle slips which is the same with the four combinations of the proposed method. We can repair MW combination cycle slips by rounding integer directly. When the threshold is larger than 0.5 cycles, we cannot repair cycle slips by rounding integer directly, and as a result, we cannot achieve the ultimate goal. Under this consideration, we set the threshold of MW as 0.5 cycles. For GF combination, the coefficients of carrier phase are not integer so we can not repair GF combination cycle slips by rounding integer simply. As a result, we respect the statistic characteristic of combined noise and set three factors of the standard deviation of the combined noise as the threshold of the GF combination. Fig 11 shows the results. As Fig 11 shows, for MW combination, there are several detection results exceeding the threshold due to the large noise; for GF combination, there is a trend component in detection results causing that many detection results exceed the threshold. As to the proposed method whose results are shown at Fig. 6, the noise is small and there is no trend component in the detection results.

2) PERFORMANCE OF TRIPLE-FREQUENCY METHOD

Liu et al. [14] proposed a triple-frequency cycle slip detect and repair method under high ionospheric activity for BDS. They constructed three linear combinations to detect and

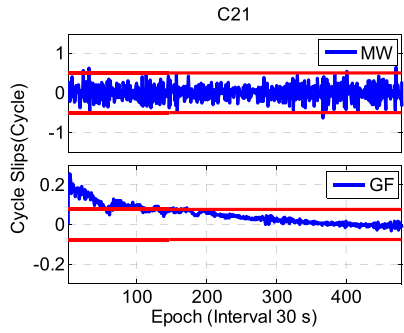


FIGURE 11. Dual-frequency detection results with sampling interval of 30 s.

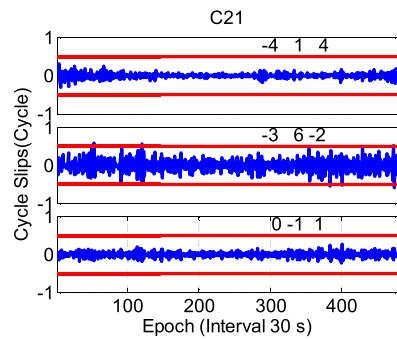


FIGURE 12. Triple-frequency detection results of (Liu et al)' method with sampling interval of 30 s.

repair cycle slips. We use BDS B1I, B2a and B3I observations to compare the performance of their method with our method. Fig. 12 shows the results. As Fig. 12 shows, Liu et al.'s method performs well during most of time. However, there exist several detection results exceeding the threshold (set as 0.5 cycles) in the second combination. As to our algorithm, there are no detection results exceeding 0.5 cycles for the four combinations. Those results further verify the effectiveness of our method. One point should be mentioned is that the threshold which Liu et al. set was three factors of the standard deviation of the combined noise and the threshold was larger than 0.5 cycles in this case. Their detection results did not exceed the threshold they set. However, they can not repair cycle slips by rounding integer directly due to threshold larger than 0.5 cycles. Detecting cycle slips is just the primary goal. Repairing cycle slips is the ultimate goal. As a result, we set 0.5 cycles as the threshold. In this way, we can not only detect cycle slip but also repair cycle slips by rounding integer directly.

F. REAL CYCLE SLIP TEST

To test the performance of the proposed algorithm, we use it to detect and repair real cycle slips using observations of BDS C20 and Galileo E08 at Changsha on April 7, 2019. Cai et al. proposed a dual-frequency cycle slip detection and repair algorithm [10]. A forward and backward moving window averaging (FBMWA) algorithm and a second-order, time-difference phase ionospheric residual (STPIR) algorithm are

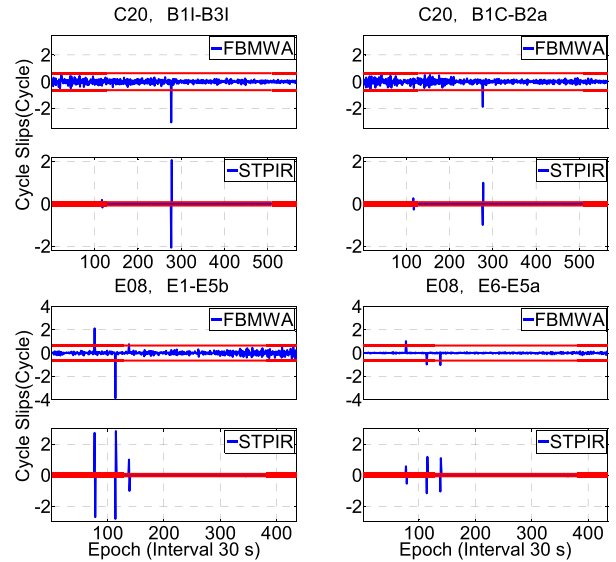


FIGURE 13. Dual-frequency detection results with real cycle slips. Top left, top right, bottom left and bottom right are C20 B1I-B3I, C20 B1C-B2a, E08 E1-E5b and E08 E6-E5a, respectively. The observation interval is 30 s.

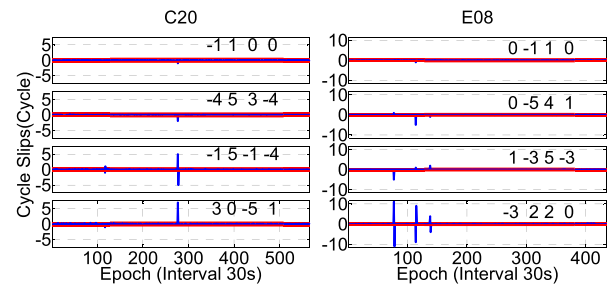


FIGURE 14. Detection results for C20 (left) and E08 (right) with real cycle slips. The observation interval is 30 s.

integrated to jointly detect and repair cycle slips in their algorithm. Their experiments show the effectiveness of their algorithm and many other researches refer to their algorithm, such as reference [16] and [18]. As a result, we use their algorithm to process the observations at first. For BDS C20, we use their algorithm to detect and repair dual-frequency cycle slip on B1I-B3I and B1C-B2a, respectively. For Galileo E08, we use their algorithm to detect and repair dual-frequency cycle slip on E1-E5b and E6-E5a, respectively. Fig 13 shows the results. We can recover dual-frequency cycle slip according to reference [10]. For expressing briefly, if dual-frequency combination is expressed as X-Y, then cycle slip pair can be expressed as (x, y), which x is cycle slip on X and y is cycle slip on Y. For BDS C20 B1I-B3I, results show that there are two cycle slips, i.e. (1, 1) at epoch 117 and (5, 2) at epoch 277. For BDS C20 B1C-B2a, results show that there are two cycle slips, i.e. (1, 1) at epoch 117 and (4, 2) at epoch 277. For Galileo E08 E1-E5b, results show that there are three cycle slips, i.e. (3, 5) at epoch 77, (5, 1) at epoch 114 and (0, 1) at epoch 138. For Galileo E08 E6-E5a, results show that there are three cycle slips, i.e. (6, 5) at epoch 77, (1, 2) at epoch 114 and (0, 1) at epoch 138. Next, we use our

algorithm to process the same observations. Fig 14 shows the results. For BDS C20, there are two cycle slip pairs. The first cycle slip pair occurs at epoch 117, and the detection results of the four detection combinations are 0.04, 0.11, -1.04 and -1.06, respectively. Then the cycle slip pair can be calculated by term (40) and it is (1, 1, 1, 1). The another cycle slip pair occurs at epoch 277, and the detection results of the four detection combinations are -0.99, -2.02, 5.01 and 6.99, respectively. Then the cycle slip pair can be calculated by term (40) and it is (5, 4, 2, 2). For Galileo E08, there are three cycle slip pairs. These three cycle slip pairs occur at epoch 77, 114 and 138, respectively. These three cycle slip pairs' detection results of the four detection combinations are (0.12, 1.02, -5.01, 11.03), (-0.99, -5.02, 0.98, -8.97) and (0.05, -1.03, 1.99, 3.95), respectively. These three cycle slip pairs can be calculated by term (41) and they are (3, 5, 5, 6), (5, 2, 1, 1) and (0, 1, 1, 0), respectively. The cycle slip detection and repair results on each frequency are the same with (Cai et al)'s algorithm, and as a result, the correctness of our algorithm in real cycle slip test is validated. Consequently, the reliability of the proposed algorithm is further tested.

IV. CONCLUSION

We propose a real-time quadruple-frequency cycle slip detection and repair algorithm based on the four chosen linear combinations in this research. Four detection combinations are determined in accordance with fixing probability in four cascaded steps. The proposed algorithm has been tested on real 30-second quadruple-frequency static observations of BDS and Galileo on April 7, 2019 and on real 0.05-second quadruple-frequency kinematic observations of BDS and Galileo on April 17, 2019. Simulated and real cycle slips are tested in the data analysis part. The results show that the proposed algorithm can detect and repair cycle slips even for one cycle under different sampling interval, i.e. 30 s and 0.05 s, and different applications, i.e. static and kinematic applications, in real time effectively. In addition, we compare the performance of the proposed method with the traditional methods. Results show that the proposed method is better than the traditional methods. Those results further verify the effectiveness of the proposed method.

REFERENCES

- [1] M. Lu, W. Li, Z. Yao, and X. Cui, "Overview of BDS III new signals," *Navigation*, vol. 66, no. 1, pp. 19–35, 2019.
- [2] *BeiDou Navigation Satellite System Signal in Space Interface Control Document Open Service Signal B31 (Version 1.0)*, China Satell. Navigat. Office, Beijing, China, 2018.
- [3] *BeiDou Navigation Satellite System Signal in Space Interface Control Document Open Service Signal B1C (Version 1.0)*, China Satell. Navigat. Office, Beijing, China, 2017.
- [4] *BeiDou Navigation Satellite System Signal in Space Interface Control Document Open Service Signal B2a (Version 1.0)*, China Satell. Navigat. Office, Beijing, China, 2017.
- [5] S. Ji, W. Chen, C. Zhao, X. Ding, and Y. Chen, "Single epoch ambiguity resolution for Galileo with the CAR and LAMBDA methods," *GPS Solut.*, vol. 11, no. 4, pp. 259–268, 2007.
- [6] J. PaziewskiEmail author and P. Wielgosz, "Assessment of GPS+Galileo and multi-frequency Galileo single-epoch precise positioning with network corrections," *GPS Solutions*, vol. 18, no. 4, pp. 571–579, Oct. 2014.
- [7] D. Chen, S. Ye, W. Zhou, Y. Liu, P. Jiang, and W. Tang, "A double-differenced cycle slip detection and repair method for GNSS CORS network," *GPS Solutions*, vol. 23, no. 3, pp. 439–450, Jul. 2016.
- [8] H. Ron, "The Synergism of GPS code and carrier measurements," in *Proc. 3rd Int. Symp. Satell. Doppler Positioning*, vol. 2, 1982, pp. 1213–1231.
- [9] G. Blewitt, "An automatic editing algorithm for GPS data," *Geophys. Res. Lett.*, vol. 17, pp. 199–202, Mar. 1990.
- [10] C. Cai, Z. Liu, P. Xia, and W. Dai, "Cycle slip detection and repair for undifferenced GPS observations under high ionospheric activity," *GPS Solutions*, vol. 17, no. 2, pp. 247–260, Jul. 2013.
- [11] Z. Liu, "A new automated cycle slip detection and repair method for a single dual-frequency GPS receiver," *J. Geodesy*, vol. 85, pp. 171–183, Mar. 2010.
- [12] S. Banville and R. B. Langley, "Mitigating the impact of ionospheric cycle slips in GNSS observations," *J. Geodesy*, vol. 87, no. 2, pp. 179–193, Feb. 2013.
- [13] R. Hatch, J. Jung, P. Enge, and B. Pervan, "Civilian GPS: The benefits of three frequencies," *GPS Solutions*, vol. 3, no. 4, pp. 1–9, 2000.
- [14] W. Liu, X. Jin, M. Wu, J. Hu, and Y. Wu, "A new real-time cycle slip detection and repair method under high ionospheric activity for a triple-frequency GPS/BDS receiver," *Sensors*, vol. 18, no. 2, pp. 427–446, Feb. 2018.
- [15] M. C. de Lacy, M. Reguzzoni, and F. Sansò, "Real-time cycle slip detection in triple-frequency GNSS," *GPS Solutions*, vol. 16, pp. 353–362, Jul. 2012.
- [16] L. Huang, Z. Lu, G. Zhai, Y. Ouyang, M. Huang, X. Lu, T. Wu, and K. Li, "A new triple-frequency cycle slip detecting algorithm validated with BDS data," *GPS Solutions*, vol. 20, pp. 761–769, Oct. 2015.
- [17] Q. Zhao, B. Sun, Z. Dai, Z. Hu, C. Shi, and J. Liu, "Real-time detection and repair of cycle slips in triple-frequency GNSS measurements," *GPS Solutions*, vol. 19, no. 3, pp. 381–391, Jul. 2015.
- [18] T. Zeng, L. Sui, Y. Xu, X. Jia, G. Xiao, and Y. Tian, "Real-time triple-frequency cycle slip detection and repair method under ionospheric disturbance validated with BDS data," *GPS Solutions*, vol. 22, no. 3, pp. 62–72, Jul. 2018.
- [19] Z. Liu and C. Wu, "Study of the ionospheric TEC rate in Hong Kong region and its GPS/GNSS application," in *Proc. Int. Tech. Meeting GNSS Global Navigat. Satell. Syst.-Innov. Appl.*, Beijing, China, 2009, pp. 129–137.



YAODING WANG is currently pursuing the Ph.D. degree with the College of Electronic Science, National University of Defense Technology, Changsha, China. His research interests include surveying data processing, cycle slip detection and repair, and GNSS precise positioning.



KE ZHANG is currently a Teacher with the College of Electronic Science, National University of Defense Technology, Changsha, China. His research interests include algorithm designs and performance analysis of global navigation satellite systems.



WENXIANG LIU is currently a Lecturer with the College of Electronic Science, National University of Defense Technology, Changsha, China. His research interests include GNSS data processing and GNSS integrity monitoring.



ZHENGRONG LI is currently a Lecturer with the College of Electronic Science, National University of Defense Technology, Changsha, China. His research interests include surveying data processing and GNSS precise positioning.



FEIXUE WANG is currently a Professor with the College of Electronic Science, National University of Defense Technology, Changsha, China. His research interests include algorithm designs and performance analysis of global navigation satellite systems.

• • •